A SEISMIC DESIGN PROCEDURE FOR DIFFERENT PERFORMANCE OBJECTIVES FOR POST TENSIONED WALLS

Enrique Hernández-Montes, Akrivi Chatzidaki, Luisa María Gil-Martin, Mark Aschheim, Dimitrios Vamvatsikos

Abstract

A method is presented for the design of unbonded post-tensioned concrete walls for seismic loading to satisfy multiple performance objectives. It takes advantage of the fact that the initial stiffness of the wall is nearly independent of the amount of post-tensioning reinforcement, and thus the fundamental period of the building can be considered to be a stable parameter in design of walls of a given cross section, independent of the degree of post-tensioning. The design spectra used follow the specification provided in Eurocode 8 considering the probability of exceedance of the seismic action. A detailed example is provided.

Keywords: Post-tensioned reinforced concrete walls, performance-based seismic design, design spectra.

1. Introduction

The model for the lateral load-displacement response of unbonded post-tensioned concrete walls proposed by Kurama et al. [1] is recognized for describing the response of this type of structure [2-5]. Kurama et al. [1] propose a design-oriented analytical model that uses a set of equilibrium equations to estimate the nonlinear static (pushover) behavior of unbonded post-tensioned (UPT) walls. The model has been verified experimentally by different researchers [2,5]. The response is characterized by five points on the pushover curve of a UPT wall representing different limit states (Figure 1). These points are: 1) DEC: decompression at the base of the wall, 2) ELL: effective limit of the linear response of the wall, 3) SPL: spalling of concrete cover at the base of the wall, 4) LLP: yielding of the post-tensioning reinforcement, and 5) CCC: crushing of confined concrete at the base of the wall. A trilinear curve can be identified linking the origin with ELL, LLP and CCC points. This trilinear curve constitutes the behavioral model proposed by Kurama et al [1].

In the case of unbonded post-tensioned precast concrete walls, mild (deformed) steel reinforcement does not connect the wall to the foundation, only the unbonded post-tensioning reinforcement crosses this interface. The initial stiffness of the wall is based on the gross or transformed section, and applies until the point that cracking and/or gap opening occur. Therefore, for a given cross-section, the contact area at the wall-foundation interface (or any horizontal plane under consideration) remains constant, and precompression (induced by gravity loads and prestress) causes every differential area to contribute to the initial stiffness of the wall, in relation to its tangent stiffness (associated with the precompression). Elongation of the unbonded post-tensioned reinforcement may be neglected in a differential lateral deformation of the wall, and thus the contribution of the post-tensioning steel to the wall stiffness is negligible. As a result, for the seismic design of buildings that utilize UPT walls as seismic-force resisting elements, the fundamental period of the building is influenced

primarily by the UPT wall cross section and is largely independent of the strength provided by means of changes in prestress level and quantity of the unbonded post-tensioning reinforcement. The unbonded post-tensioning steel is anchored at the top of the wall and places the wall fully in compression. Because the steel is unbonded, the stiffness of the wall before decompression is determined by the properties of the concrete. As a result, the stability of the period (T) in this case makes it the best variable to use in the seismic design process, whereas for many other systems, the yield displacement is a more stable and hence preferable parameter to use in seismic design [6,7].

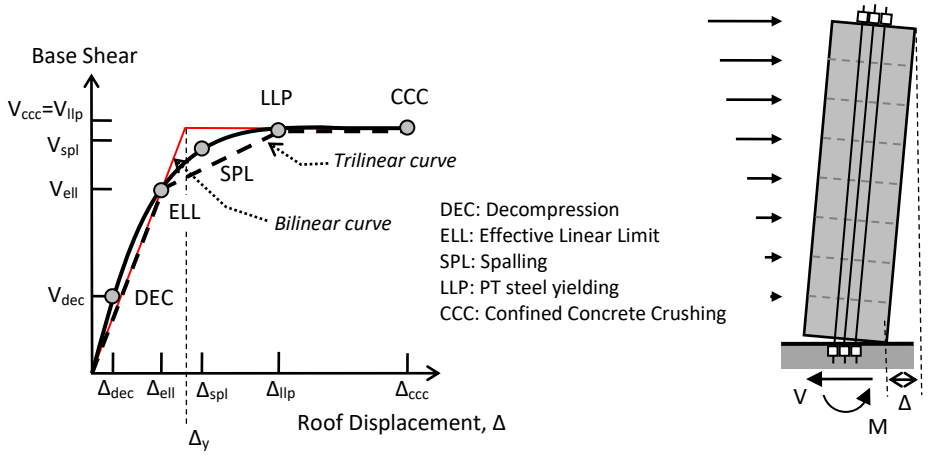

Figure 1. Generic capacity curve determined by nonlinear static (pushover) analysis of an unbonded post-tensioned wall

The ductility of the system, and the so-called behavior factor in the case of Eurocode notation [8], are referenced to the definition of yield displacement. A bilinear approximation of the pushover curve of the UPT wall can be constructed with the values of V_{ell}, Δ_{ell} and V_{llp}, allowing an effective yield displacement, Δ_y, to be defined as shown in Figure 1.

Example Part 1

The design method is illustrated by an example composed of several parts. Figure 2 shows a cast-in-place UPT reinforced concrete wall that is part of a 4-story reinforced-concrete (RC) structure. The height of the first story is 5 m while the overlying stories are 4 m high, resulting in a total height of 17 m. The building has two post-tensioned walls in each principal direction. The walls indicated in Figures 2 and 3 will be designed according to Eurocode 8 (EC-8) [8], and Eurocode 2 (EC-2) [9]. Each consists of a rectangular section having a plan length of 6.0 m and thickness of 0.5 m. B500 steel reinforcement (f_{yk}=500 MPa) and C-30 concrete (f_{ck}=30 MPa) are used. The material safety factors used in the design are γ_s=1.0 and γ_c=1.0.

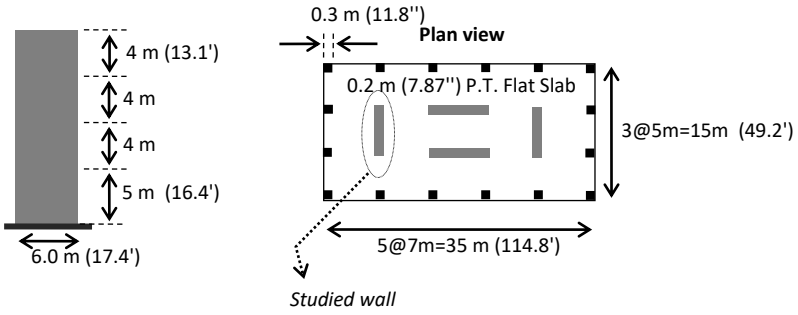

Figure 2. Unbonded post-tensioned reinforced concrete wall.

The transverse hoops in the boundary zones at the ends of the wall section are of 12-mm diameter at vertical spacing of 100 mm. According to the Mander model [10] they provide confinement, allowing the confined core concrete to develop a compressive strength of $f_{cc} = 47.85$ MPa (based on characteristic values) at strain $\varepsilon_{cc} = 0.0079$ and with an ultimate strain of $\varepsilon_{cu} = 0.044$. As shown in Figure 3, the wall contains five bundled tendons. Each tendon consists of some number of individually greased and sheathed seven-wire strands; the precise quantity is to be determined based on the seismic performance objectives and site seismicity.

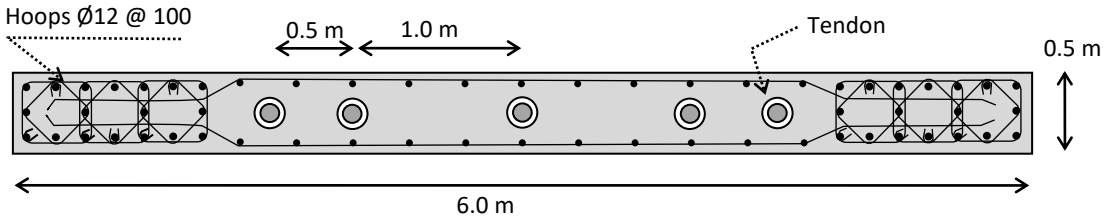

Figure 3. Initial configuration of the unbonded post-tensioned wall. A cover of 25mm is assumed, while the confined area is 135x45mm at each edge.

The five tendons are considered to be of the same cross-sectional area. Table 1 shows the values of V_{ell}, Δ_{ell}, V_{llp} and Δ_y for different values of the tendon cross-section.

Table 1. Points defining the bilinear curve.

Strands per tendon	Tendon area (mm^2)	V_{ell} (kN)	Δ_{ell} (mm)	V_{llp} (kN)	Δ_y (mm)
15	2100	2346	10.0	3525	15.1
20	2800	2847	12.2	4319	18.5
25	3500	3270	14.0	5007	21.4

Figure 4 shows the bilinear curve computed for the UPT wall (the cross section of Figure 3 for the 4-story building of Figure 2). In all cases, the PT is prestressed to $0.55f_{pu}$, where f_{pu} is the nominal ultimate strength of the prestressing steel. Although the strength is controlled by the PT steel, the stiffness is determined primarily by the geometry of the wall and elastic modulus of concrete and thus the stiffness of the curve in the linear range varies little. This fact suggests

that the seismic design of this type of lateral systems will converge rapidly if based on an assumed period, for a wall of a given section. Of course, the cross-section may be revised if the structure is too flexible or overly stiff. As a first approximation:

$$T = 2\pi\sqrt{\frac{m}{k}} = 0.34\ s \tag{1}$$

where m is the reactive mass tributary to the wall and k is the stiffness defined by the slope in the linear range of the curves in Figure 4. The tributary dead load in combination with 25% of the live load result in a tributary mass per wall of 722 ton. Of course, since the mass is distributed over the height of the building (rather than being lumped at the top), the period of the building will be less than that given in Eq. 1. Using a distributed plasticity (fiber) model, with the commercial software SeismoStruct© [11], a first-mode period of 0.31 s was obtained, instead of the 0.34 s given by Eq. 1.

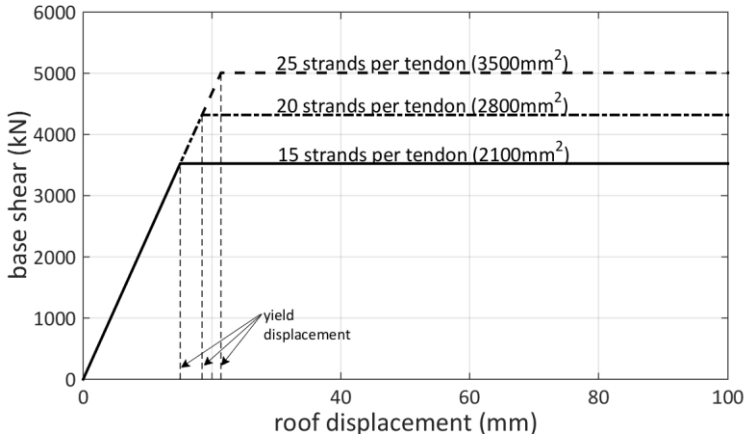

Figure 4. Influence of area of post-tensioning reinforcement on the stiffness and strength of an unbonded post-tensioned wall using a simplified bilinear curve to characterize the response.

2. Eurocode 8 compatible design spectra in terms of probability of exceedance.

Eurocode 8 [8] presents two types of spectra (Type 1 and Type 2) and for each, five types of site (ground) conditions can be considered. Given the type of spectra and the site (ground) classification, EC-8 Tables 3.2 and 3.3 provide the values of S, T_B, T_C and T_D that are used to define the design spectrum. The design ground acceleration, a_g, and a damping factor are also considered (e.g. η=1 for 5% damping). These values define the design spectrum $S_d(T, q)$ for a given site as a piecewise function of period T and the behavior factor q, where S_d is the design spectral acceleration (m/s^2).

Performance-based seismic design can consider different limit states (performance) occurring under various intensities of ground shaking. Ground shaking intensity is indexed by the probability of exceedance, which may be specified as, for example, an intensity which has probability of 10% of being exceeded in a 50-year interval. Different limit states can be

associated with applicable probabilities of exceedance, leading to one or more seismic performance objectives. Eurocode 8 defines $S_d(T, q)$ for an event with a probability of exceedance of 10% in 50 years (equivalent to shaking intensity that has a mean return period of 475 years) for use in design in conjunction with a defined ductility factor, given by q. Eurocode 8 restricts interstory drift limits for a less intense (and more frequent) shaking intensity, having approximately a 10% probability of exceedance in 10 years (a mean return period of 95 years). The adjustment of shaking intensity to account for the change in mean return period is implemented in Eurocode 8 through the importance factor, γ_I.

The design ground acceleration a_g, considered above, is equal to the reference peak ground acceleration on type A ground (associated with the site), a_{gR}, multiplied by the importance factor γ_I ($a_g=\gamma_I a_{gR}$). While the EC-8 design spectra are defined for an event with a probability of exceedance of 10% in 50 years, EC-8 (Note to §2.1(4)) allows extrapolating the design spectra to different probabilities of exceedance by assuming a linear approximation of the hazard curve in log-log coordinates (Cornell et al. [12]):

$$H(s) = k_0 \cdot s^{-k} \tag{2}$$

where *s* is the intensity measure of choice, and H(s) the corresponding mean annual frequency (MAF) of exceedance. Due to the underlying Poisson assumption, the MAF can also be expressed via the probability *p* of exceeding a given value of intensity s over a period of 50 yr as

$$H(s) = -\frac{\ln(1-p)}{50} \tag{3}$$

This allows us to define a scaling factor, γ_p, similar to the importance factor of EC-8, to estimate a design spectrum for a different probability of exceedance (p) compared with the standard 0.1 (or 10%), over a period of 50 years:

$$\gamma_p = \left[\frac{\ln(1-p)}{\ln(1-0.1)}\right]^{-\frac{1}{k}} \approx \left(\frac{p}{0.1}\right)^{-\frac{1}{k}} \tag{4}$$

where k depends on the site seismicity, with values of the order of 2 – 4 suggested by EC-8 for Europe. Herein, k = 3 is employed. Note that the simplification appearing in the final part of Eq. (4) is based on the first-order Taylor approximation of $\ln(1-p) \approx p$ that only holds for $p \ll 1$. Still, for practical purposes it is deemed accurate enough up to p=0.5, as the error is only 10%. Then, simply by multiplying by γ_p one can modify the design spectra defined for a 10% probability of exceedance in 50 years to a probability of exceedance of p in 50 years. Thus, the design spectral acceleration can be expressed as a function of 3 variables (T, q, and p).

$$S_d(T, q, p) = \gamma_p \, S_d(T, q) \tag{5}$$

Example Part 2

The hazard for the site is described by a Type 1 design spectrum, defined by EC-8 for sites characterized by events with a surface-wave magnitude (M_s) greater than 5.5. The site conditions in this example are described by a soil type B and a peak ground acceleration a_{gR} of 0.3 g. Figure 5 provides a 3-dimensional illustration of the EC-8 design spectrum, $S_d(T,q,p)$, as function of the probability of exceedance, p, in a 50-year time interval, and the fundamental period, T, of the structure, for two values of the behavior factor, q= 1 and 2.

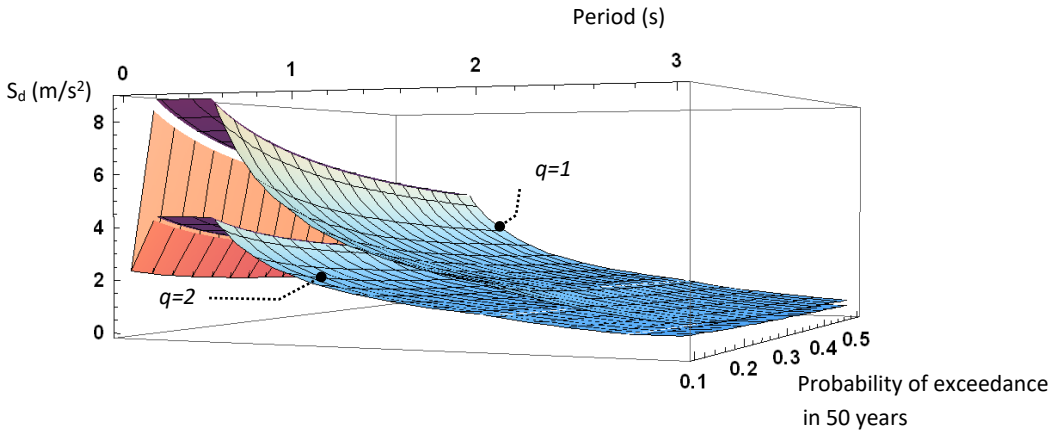

Figure 5. EC-8 design spectra type 1, soil B, a_{gR}=0.3g . Tϵ[0,3] and pϵ[0.5,0.1]. q=1 and q=2.

Different 2D representations of the spectra shown in Figure 5 can be created. For example, classic elastic design spectra (q=1) for different exceedance probabilities appear in Figure 6:

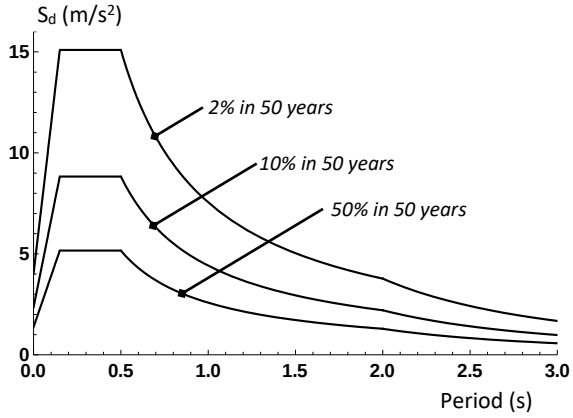

Figure 6. EC-8 design spectra for different exceedance probabilities based on Figure 5.

For the case in which T may be assumed constant during the design process, as may be assumed for UPT concrete walls, plots of S_d as function of q and p for a fixed value of T are of interest. The design spectral acceleration for T=0.31 s as function of q (and for different values of p) for this example is given in Figure 7.

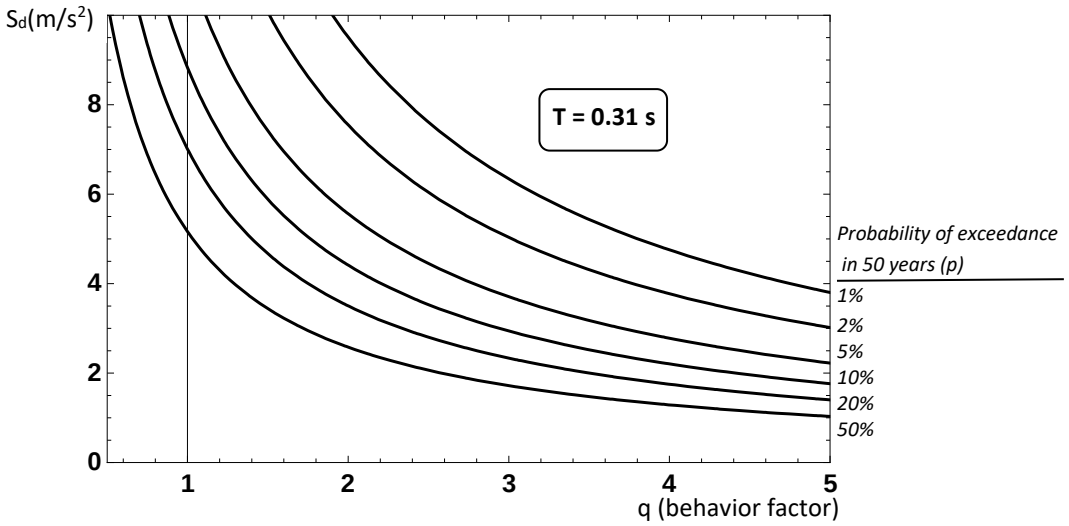

Figure 7. S_d as function of q and p for a constant value of T=0.31 s.

3. Design method for multiple performance objectives

To illustrate the design of a UPT wall we select three performance objectives (POs), each defined [13] by (i) the exceedance of a specific limit-state (LS) that bears consequences for the building (structural/non-structural components and contents), (ii) a maximum allowable mean annual frequency (MAF) of exceedance, which designates how often this LS can be violated, and (iii) a confidence level, that determines how confident we wish to be regarding the exceedance (or non-exceedance) of the aforementioned MAF given the inherent uncertainties in the problem (e.g. due to model type, material properties, analysis approach etc.). The three performance objectives are:

1. PO_1: Effective yield for an event with a probability of exceedance of 50% in 50 yr (p=0.5, return period of 72 yr) at a confidence of 50% (essentially disregarding the influence of additional uncertainties). This limit state is somewhat beyond the point at which softening has developed as a result of the progression of gap opening and nonlinearity in the response of concrete in compression. However, as an approximation, both concrete and steel materials can be considered to be essentially elastic up to this point; spalling of cover concrete would be anticipated at somewhat larger displacements.

2. PO_2: An interstory drift limit having a probability of exceedance of 20% in 50 yr (return period of 224 yr) at a confidence of 65%. This represents a serviceability limit state similar to the one specified in EC-8, yet at the same time considerably stricter, as the EC-8 employs a less strict MAF of 10% in 10 years (95 yr return period). For this example, we adopt an interstory drift limit of 0.7% of the story height. Note that since the period is largely independent of the strength, and thus the tendon area, if this limit-state is found to govern, then the UPT-wall section

dimensions may need to be enlarged. A new "constant" period will have to be estimated and the process restarted.

3. PO_3: The limit of response associated with crushing of the confined core (CCC behavior in Figure 1). We consider this simply as a point of incipient collapse, although the true sequence of events heralding collapse may be much more complicated. Following ASCE/SEI 7-10 [14] we assign a probability of 1% in 50 years, adding a high confidence of 90% due to the considerable consequences associated with this limit-state.

The design method is expressed in the flowchart of Figure 8. Note that the proposed approach is uncertainty-agnostic; therefore, confidence is not accounted for in design, but is accounted for in assessment, and thus in any subsequent corrective iterations. The performance objectives are translated into equivalent values of q. We assume that the effective yield displacement, identified in Figures 1 and 4, corresponds to a behavior factor q=1, and that the strength required with this performance objective may control the design. Once this strength is determined, the associated yield displacement and the ductility values corresponding to the other limit states may be determined, and the adequacy of the preliminary design may then be assessed for this limit state. A detailed performance assessment can be made to evaluate the first design realization; if needed, the design can be iteratively improved.

Given the value of the natural period T, q=1, and p=0.5, the design pseudo-acceleration S_{d1} can be determined (Eq. 5) and the corresponding base shear can be calculated. A first-mode-compatible or an inverted-triangular distribution (per Eurocode 8) of external horizontal forces can be applied. This force level corresponds to the yield strength of the wall observed in a nonlinear static (pushover) analysis. Thus, the UPT wall is designed for flexural strength and base shear strength corresponding to V_{llp}. Once the PT reinforcement is designed, Δ_{ell}, V_{ell}, Δ_y, V_{llp}, Δ_{llp}, Δ_{ccc} are calculated, thereby allowing compliance with the other performance objectives (limit states) to be confirmed. We have assumed in this iteration that the first performance objective governs the design of the structure.

To evaluate satisfaction of the other performance objectives at this preliminary stage, the interstory drift limit and collapse displacement are expressed in terms of the ratio of peak roof displacement corresponding to each objective and the effective yield displacement. This ratio, considered equal to the behavior factor (EC-8 §4.3.4 (1)), is given as q_2 = (Drift limit)/Δ_y and $q_3 = \Delta_{ccc}/\Delta_y$. The associated 50-year probabilities of exceedance, $p = 0.2$ and $p = 0.01$, respectively, were identified for the performance objectives stated above. As pointed out in the previous paragraph we have assumed that the values of pseudo-acceleration corresponding to these behavior factors, S_{d2} and S_{d3}, do not govern the design; however, if S_{d2} or S_{d3} are greater than S_{d1}, the design may be revised using the largest value of pseudo-acceleration, as indicated in Figure 8. If S_{d2}, i.e., the drift limitation, is found to govern, the dimensions of the UPT-wall section may need to be enlarged.

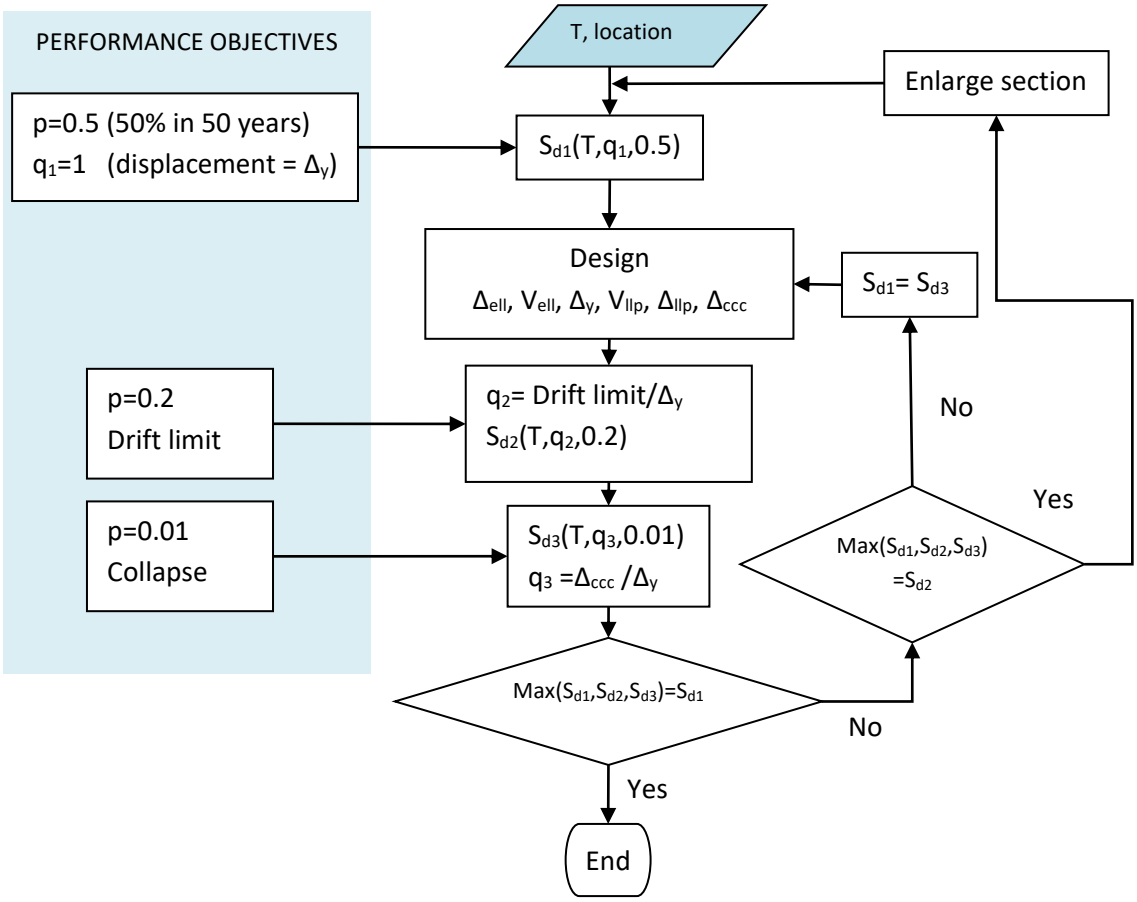

Figure 8. Flowchart of the design method.

Example Part 3

The first performance objective is defined for q=1, corresponding to the effective yield displacement, Δ_y, and an associated probability of exceedance of 50% in 50 years (p=0.5). Using Eq. 5 or its graphical representation in Figure 7, we find the value of $S_d(T,q,p)= S_d(0.31,1,0.5)=5.16$ m/s^2. The corresponding base shear is $V_b=S_dm=3723$ kN. According to the models described in [1,2], the design base shear strength ($V_{llp}\approx V_b$) is achieved using 17 seven-wire strands per tendon, for which $\Delta_{ell}=10.9$ mm, $V_{ell}=2558$ kN, $\Delta_y=16.5$ mm, $V_{llp}=3856$ kN, $\Delta_{llp}=386$ mm and $\Delta_{ccc}=584$ mm. To account for differences between test results and the estimate of the Mander et al. [10] model for the confined concrete crushing strain, ε_{cu}, a reduction factor of $\psi=0.9$ is employed [2], reducing the estimated value of ε_{cu} = 0.044 to 0.04.

For such a stiff system, we assume that interstory drifts are dominated by rigid body rotation of the wall about the base (associated with gap opening behavior at the base). Thus, the interstory drift limit of 0.007 corresponds to a drift of 119 mm at the roof. The resulting behavior factor is $q_2 = 119\text{mm}/16.5\text{mm} = 7.2$. The limit state of crushing of the confined concrete corresponds to a behavior factor $q_3 = 584/16.5 = 35.4$. The values of pseudo-acceleration corresponding to these behavior factors for the site of interest are shown in Figure 9, and they are found to be:

$$S_{d2}(0.31, 7.2, 0.2) = 0.97 \ m/s^2$$
$$S_{d3}(0.31, 35.4, 0.01) = 0.54 \ m/s^2$$

The largest S_d value of the three, namely the one corresponding to the effective yield, obviously controls the design, as initially assumed. Therefore, no revision of the preliminary design is required. The idealized load-displacement response of the resulting wall, according to the model proposed by Kurama et al. [1] and Pérez et al. [2], is shown in Figure 10.

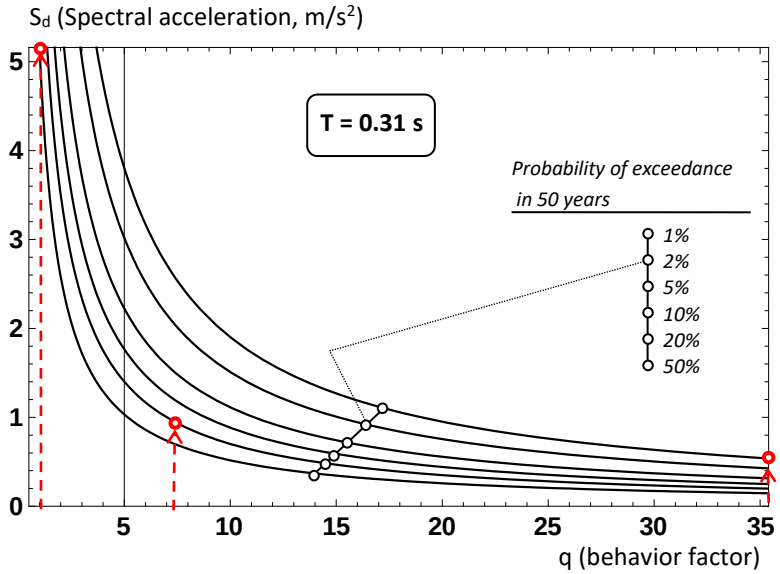

Figure 9. Determination of S_d for the three performance objectives considered. The effective yield limit (q=1) obviously produces the highest S_d requirement and thus governs.

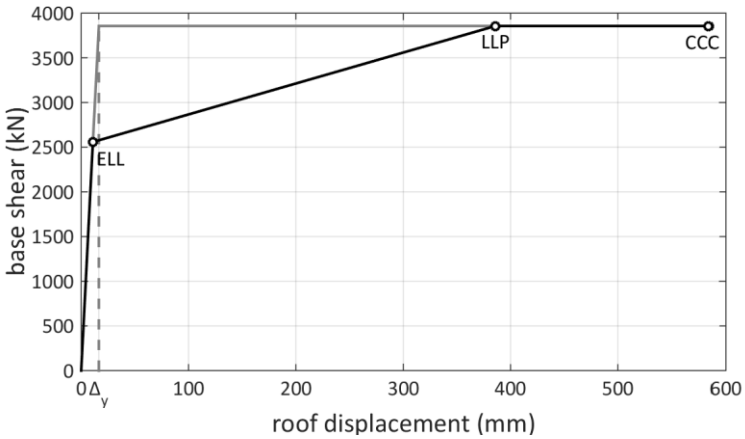

Figure 10. Trilinear idealization of the response of the unbonded post-tensioned wall, as determined by preliminary design.

4. Assessment and Validation

A two dimensional model of one of the two identical post-tensioned walls that act in each direction was prepared using OpenSees [15] to assess the performance of the design. The post-tensioned wall was modelled following the suggestions of Buddika and Wijeyewickrema [16] as shown in Figure 11. A single displacement-based distributed plasticity element was employed for each story, with fiber section representation monitored at five integration points along the member length. Further discretization of the wall along its height into more displacement-based elements, or the use of force-based elements (which are often important for improved accuracy [17]), was not found to be necessary as nonlinearity is concentrated at the rocking base, away from the wall elements. At the top and bottom, rigid beams were employed to define the outline of the wall. The unbonded tendons were modelled using tension-only corotational truss elements connected to a rigid top and to the foundation. At the bottom, in order to model rocking, the rigid wall base running along the entire width of the wall is connected with no-tension concrete-like springs to the foundation (Figure 11a). The leaning column was modelled as pinned at its foundation and continuous through its height, using linear elastic elements. These have area and moment of inertia characteristics that match the corresponding cross-sectional properties of one half of the gravity columns of the building plus one post-tensioned wall oriented along the transverse direction bending around its weak axis, as only one-half of the building is modeled in the direction of interest due to symmetry. A first-order treatment of geometric nonlinearities was also incorporated to account for global P-Delta effects. Rayleigh damping of 2% was assigned to the first and second modes. This is lower than a typical value of 5% for reinforced concrete structures, but it is considered realistic as cracking is directly incorporated in the concrete material models (giving rise to early hysteretic damping) both at the base and in the wall itself.

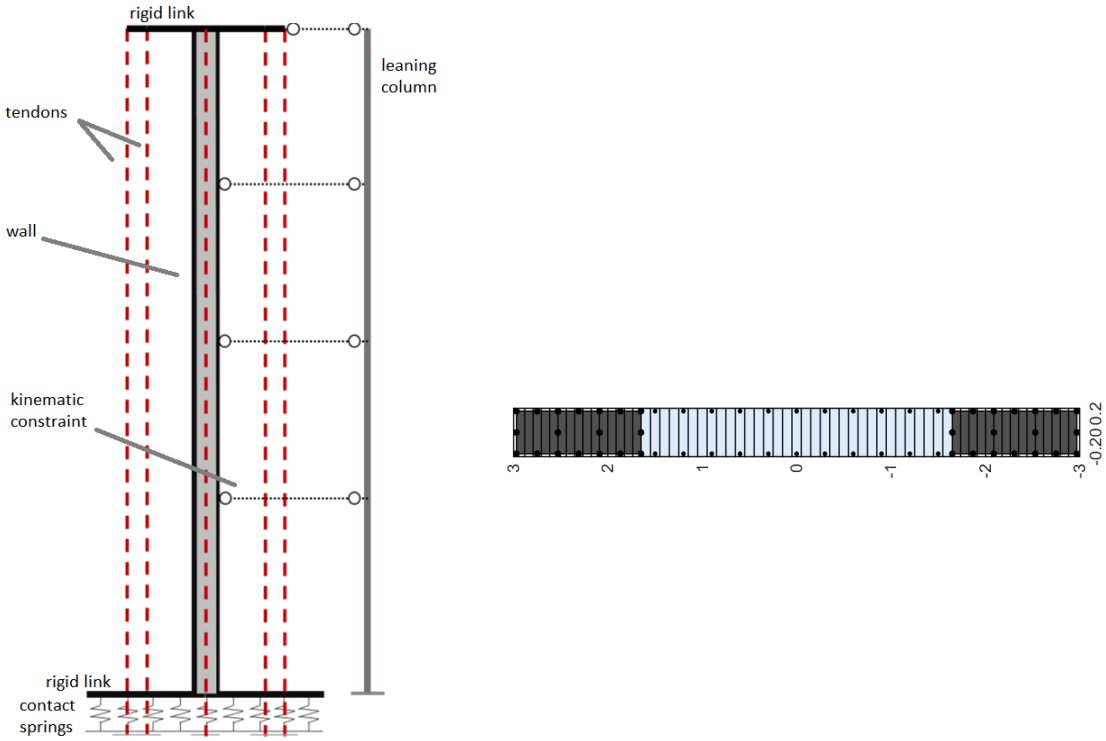

Figure 11. OpenSees model of: (a) the building showing the wall (grey-black rectangle), the tendons (dashed red), the leaning column (dark grey), the contact springs, the rigid links (solid black), and the horizontal kinematic constraints (dotted black); (b) the post-tensioned wall

section, showing discretization into confined concrete (dark gray), semi-confined/unconfined concrete (light gray) and steel (black) fibers.

The wall section was discretized into longitudinal steel and concrete fibers, the latter having different confinement factors for the cover, the well-confined core at the edges and the semi-confined core of the web (Figure 11b). The effect of confinement was calculated on the basis of the Mander et al. model [10] with a resulting confinement ratio (f_{cc}/f_{ce}) of 1.55 for the edge core concrete (per Figure 3 detailing, based on expected material properties), 1.1 for the web core concrete (assuming typical low transverse reinforcement) and 1.0 for the unconfined cover. Steel reinforcing bars were modelled using a bilinear constitutive law accounting for pinching and stiffness degradation. Expected (denoted by subscript "e"), rather than characteristic (denoted by subscript "k"), material properties were used for both materials, i.e., a concrete strength of $f_{ce} = f_{ck} + 8 = 38$ MPa [9] and a rebar steel yield strength of $f_{ye} = 1.15f_{yk} = 575$ MPa. The base contact springs were arranged as a single stripe along the 6m width of the wall; no further discretization is required along the wall thickness in 2D. They were assigned a force-displacement relationship that mimics the hysteresis of the corresponding core concrete fibers in compression, whereby the force response is defined by the concrete stress multiplied by the relevant tributary area, while the corresponding deformation is derived by the concrete strain times an effective height of twice the confined thickness of the wall, following the recommendations of Perez et al. [2]. Each unbonded tendon has an area equal to (17 strands)·(140 mm^2/strand) = 2380mm^2. For the prestressing steel, a bilinear constitutive law was employed, with initial strain iteratively calculated to attain the initial pretension force of the tendons. The expected strand properties were determined according to JCSS [18]: Ultimate strength of $f_{pe} = f_{pk} + 66$ MPa = 1926 MPa and Young's modulus of $E_p = 195$ GPa. The ultimate strain of tendons was considered to be equal to 0.02, which may be conservative but does not govern incipient collapse.

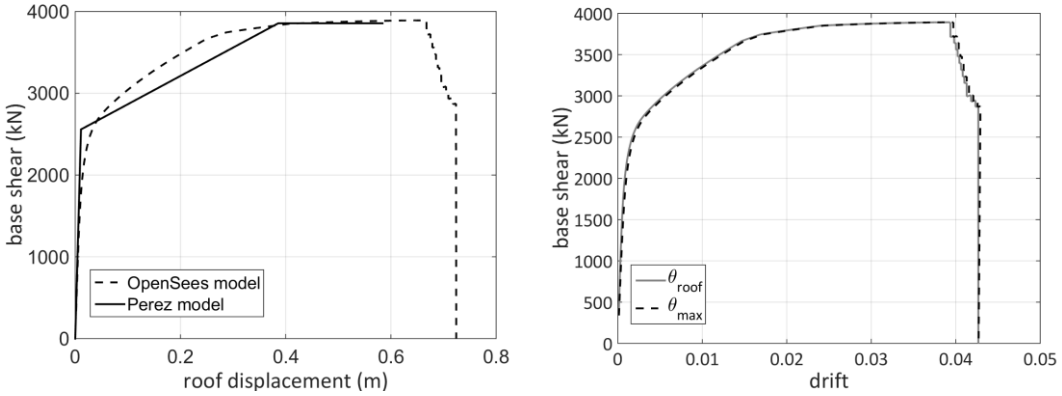

Figure 12. Static pushover capacity curves of the post-tensioned wall model: (a) Pushovers in terms of roof displacement, as created using OpenSees with expected material properties (dashed line) and via the Perez et al. [2] analytical expressions for characteristic material properties (solid line). (b) The OpenSees model pushover in terms of ϑ_{max} and ϑ_{roof}; there is negligible difference between the two due to the rigidity of the wall.

The eigenvalue analysis of the model showed that the first two modes vibrate at $T_1 = 0.28$ s and $T_2 = 0.04$ s, fairly close to the earlier estimates of $T_1 = 0.34$ s from Eq. 1, or $T_1 = 0.31$ s from the preliminary Seismostruct model. The difference with the latter can be attributed to the leaning column stiffness that is not accounted for in the preliminary estimate. The static pushover capacity curve of the model resulting from a first-mode-proportional lateral load pattern is presented in Figure 12a, along with the trilinear curve used for the design of the building,

determined from the Perez et al. [2] analytical expressions. As mentioned earlier, expected material properties were used for the former and characteristic ones for the latter case, thus the two pushover curves may seem to match perfectly for this building, yet only under somewhat different initial assumptions. Figure 12b also shows the obtained pushover response in terms of the maximum interstory drift ratio, ϑ_{max}, and the maximum roof drift ratio, ϑ_{roof}, confirming that the rigid-body rotation of the wall around its compression toe dominates the response, allowing no concentration of deformations in any individual story.

The seismic performance of the structure was evaluated using incremental dynamic analysis (IDA, [19]). Analysis results are characterized by two scalars, an Intensity Measure (IM), which represents the seismic intensity of the record, and an Engineering Demand Parameter (EDP) which monitors the structural response of the model. The first-mode spectral acceleration, $S_a(T_1,5\%)$, was adopted here as the IM, while ϑ_{max} and ϑ_{roof} were used as the EDPs. Due to considerable record-to-record variability, IDA requires a large enough set of records to cover the full range of structural response. For this reason, the 2D model of the structure was subjected to 44 natural ground motion records (22 seismic events, two components each) comprising the FEMA P695 far-field set [20].

In order to estimate the mean annual frequency (MAF) of exceeding (i.e. violating) the limit-state (LS) associated with each performance objective (PO), two components are needed: (i) the building fragility curve associated with the LS and IM of interest and (ii) the seismic hazard curve for the IM. A fragility curve is a continuous function of the IM, P (D > C | IM), that given the level of the IM provides the probability of seismic demand, D, exceeding the seismic capacity (or threshold), C, that signals violating the LS. Fragilities are typically assumed to follow a lognormal distribution, fully defined by its median value and dispersion (standard deviation of the log-data) β. The seismic hazard curve, λ(IM), of a given site relates values of the IM of interest with their MAF of exceedance. The MAF of exceeding a given limit-state, λ(D>C) is calculated by convolving the seismic hazard curve with the fragility curve [19]:

$$\lambda(D>C) = \int P\left(D>C \mid IM\right) \cdot \left|\mathrm{d}\lambda\left(IM\right)\right| \tag{6}$$

where $|\mathrm{d}\lambda(IM)|$ is the differential of the seismic hazard curve. In mathematical terms, meeting a PO means that the x% percentile estimate (due to additional uncertainty from modeling, analysis, material properties etc.) of $\lambda(D>C)$ should be lower than the associated maximum tolerable MAF of λ_{PO} [13]:

$$\lambda_{x\%}(D>C) < \lambda_{PO} \tag{7}$$

where x% is the desired confidence level at which the PO should be met. For example, for PO_1 we have x = 50% and $\lambda_{PO} = -\ln(1-0.5)/50 = 0.0139$ (corresponding to 50%/50yr).

The seismic hazard curve used for the assessment of the structure is derived for San Jose, California (latitude = 37.33659 and longitude = -121.89056) based on USGS data. In order to offer a fair assessment of the design methodology without bias due to a spectrum mismatch, the seismic hazard curve was modified (i.e., uniformly scaled) so that at MAF = −ln(1−0.10)/50 = 0.0021 (i.e., 10%/50 years) it matches the spectral acceleration calculated from the design spectrum. The resulting (modified) hazard curve derived for the post-tensioned wall is presented in Figure 13a. The dashed line indicates the approximation of the slope of the hazard curve (k=3) that was used in the design process. In Figure 13b, actual Uniform Hazard

Spectra (UHS) for the site are compared against the corresponding spectra that were extrapolated from the code design spectra via Eq. 5. It can be seen that for the fundamental period of the building, the adopted (modified) UHS matches well with the EC-8 design spectrum of 10%/50yr. For other MAFs, the approximation of k=3 led to conservative design spectra, as the S_a values that were estimated are greater than those that we would get from the actual hazard. This is a natural consequence of the power law approximation of the hazard via Eq. 2, and can only be alleviated if the actual UHS are available to be used in place of the approximate EC-8 derived spectra.

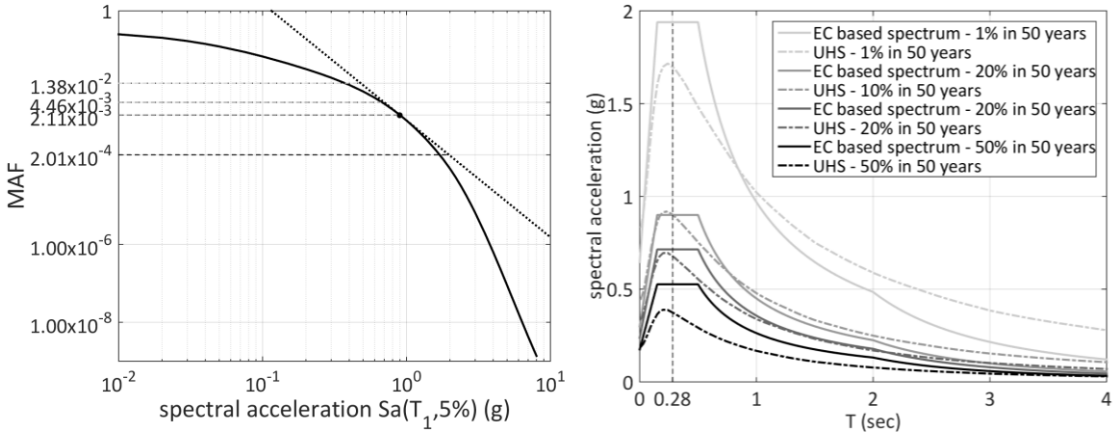

(a) (b)

Figure 13. a) Seismic hazard curve for T_1=0.28 s at San Jose CA scaled to match the 10%/50 yr value of $S_a(T_1)$ as provided by the design spectrum, and a first-order fit approximation with k=3 in the vicinity of S_a = 0.9g and b) UHS plotted against the EC-8 based design spectra for different MAFs.

Table 2. Verification of performance objectives.

Performance Objective	PO_1: Effective yield	PO_2: ϑ_{max}= 0.7%	PO_3: Crushing of confined concrete
Fragility curve (median / dispersion)	0.41g / 22%	1.07g / 37%	3.68g / 48%
Additional uncertainty (dispersion)	25%	25%	25%
Estimated MAF (yrs^{-1})	0.0128	0.0025	0.000159
Allowable MAF (yrs^{-1}) (probability / years)	0.0139 (50% / 50yrs)	0.0045 (20% / 50yrs)	0.000201 (1% / 50yrs)
Confidence level	50%	65%	90%
Check	✓	✓	✓

Results for each performance objective are summarized in Table 2. The first two values for each PO correspond to the median and the dispersion of the lognormal fit of the fragility curve, the latter due to record-to-record variability only. Then comes the dispersion due to additional uncertainties, where we essentially assume that any uncertainties other than record-to-record variability cause the fragility median to be lognormally distributed with a log-standard deviation of 0.25 (the so-called first-order assumption [12]). The following two values are the estimated

MAF (at the designated confidence level) and the allowable MAF against which the former is compared.

The acceptability of the effective yield of the building was assessed at the 50%/50yr level. This PO is equivalent to a roof displacement of Δ_y=16.5mm. This value is estimated using the Perez et al. [2] analytical expressions and agrees well enough with the results that we get from the pushover curve. The MAF of exceeding ϑ_{roof} = 16.5mm/17000mm = 0.00097 was estimated using the log-normal fragility curve fitted to the $S_a(T_1,5\%)$ values that correspond to the roof drift limit (light blue points in Figure 14a). The median value of the lognormal distribution equals 0.41g and the log standard deviation is 22%. The estimated MAF of exceeding ϑ_{roof} = 0.00097 at 50% confidence is 0.0128, which is marginally lower than the limit of − ln(1 − 0.5)/50 = 0.0139 (corresponding to 50%/50yr). Note that this small difference in MAFs corresponds to an even smaller difference in terms of $S_a(T_1)$ due to their exponential relationship. Thus, only a small margin of safety has been achieved despite the large conservatism in the assumed 50%/50yr design spectrum relative to the actual UHS observed in Figure 13b. The main reason is that the preliminary design approach neglects the effect of fragility dispersion (either due to record-to-record variability or due to modeling and analysis), which is fully accounted for in assessment. This is known to adversely increase the demand MAF [12] by factors that may range from 1.5 to 3. In the case at hand, the initial conservatism due to the power law approximation of the hazard curve happened to offset the unconservative effect of neglecting dispersion. Still, this situation may be reversed for another site or building case, or even with different PO definitions. For example, had we requested an increased confidence of, say, 65% in meeting PO_1, a redesign would probably be required as the present design approach cannot account for the higher confidence. Still, this would only require a small correction, i.e. an increase in tendon area, as the initial design has already brought us very close to fully satisfying all requirements.

For PO_2 and PO_3 (i.e. interstory drift ratio of 0.7% and crushing of confined concrete), ϑ_{max} is used as the EDP and the IDA results are shown in Figure 14b. The fragility curve for PO_2 was calculated based on the $S_a(T_1,5\%)$ values that correspond to the 0.7% interstory drift ratio limit (Figure 14b, light blue points). The median value of the lognormal distribution is equal to 1.07 g and the log standard deviation is 37%. Applying Eq. 6, the estimated mean annual frequency of exceeding the maximum interstory drift limit of 0.7% at 65% confidence is 0.0025, which is lower than the targeted MAF value of 0.0045 (or 20%/50 yrs). Thus, PO_2 is satisfied.

Crushing of confined concrete is deemed to occur when numerical non-convergence appears, or a maximum interstory drift of 4.3% is exceeded, whichever occurs first. The first criterion is *numerically* indicative of global dynamic instability [19], closely corresponding to the catastrophic loss of strength appearing at the end of the plateau in the pushover curve of Figure 12a. The second criterion corresponds to an interstory drift that is *physically* consistent with the loss of strength in the pushover analysis (Figure 12b), used to guard against any excessive deformations due to some low residual strength that may appear. Herein, the second criterion nearly always governed, and the corresponding values of $S_a(T_1,5\%)$ are employed to define the fragility curve for PO_3 (Figure 14b dark blue points). Their median value equals 3.68g and the log standard deviation is 48%. By convolving with the hazard curve of Figure 13a, the estimated MAF at 90% confidence equals 0.000159, which is lower than the required target of 1%/50 yr, or 0.000201, meeting the performance objective. Note that, in general, this MAF estimate for global collapse is conservative, as the simple amplitude scaling that IDA employs and the use of $S_a(T_1,5\%)$ as the IM may not allow for capturing the appropriate spectral shape of high intensity ground motions [21, 22]. Specifically, FEMA P-695 [20] recommends employing a spectral shape factor, to adjust the median collapse IM capacity

upwards. Although this remains a crude approximation and better methods do exist for achieving unbiased assessment of global collapse (e.g., see Lin et al. [23], Kazantzi and Vamvatsikos [24], Adam et al. [25], Kohrangi et al. [26]), this factor can be used to refine the estimate of collapse capacity, and improve the estimated margin of safety if needed.

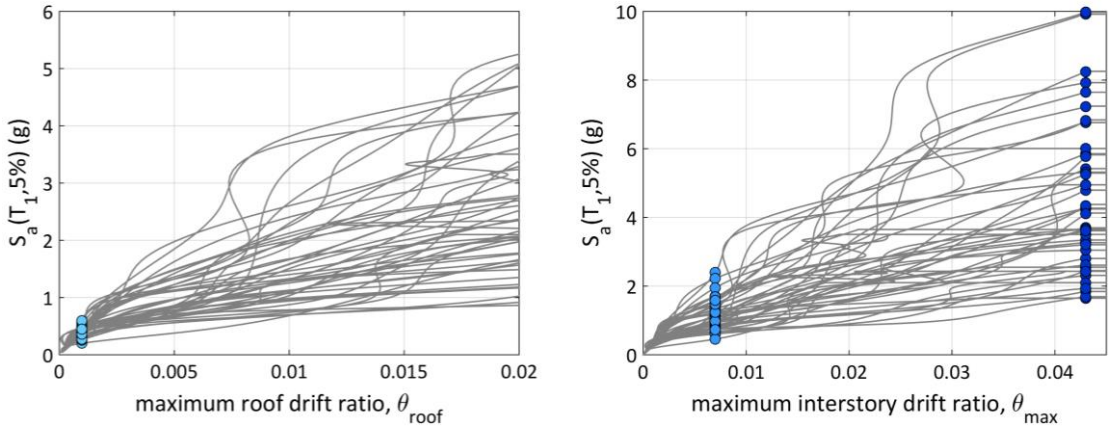

(a) (b)

Figure 14. IDA curves for estimating mean annual frequency of exceeding each PO: a) the $S_a(T_1,5\%)$ values calculated for ϑ_{roof} = 0.00097 (light blue points – PO_1) and (b) the $S_a(T_1,5\%)$ values calculated for ϑ_{max} = 0.7% (blue points – PO_2) and for crushing of confined concrete, i.e., incipient collapse (dark blue points – PO_3).

Conclusions

A seismic design procedure for the performance-based design of unbonded post-tensioned reinforced concrete walls is illustrated. The seismic action uses the EC-8 design spectra in terms of probability of exceedance. Multiple performance objectives are addressed, using a constant period assumption and relying on an accurate assessment of the performance of the resulting building to verify compliance.

The proposed method offers an initial design close to the desired one, while employing some approximations for reasons of simplicity. Specifically, it relies on a linear fit (in natural log space) of the hazard curve within the range of interest. This fit introduces some conservatism to the process as it over-represents the influence of both more frequent and rarer events. Furthermore, record-to-record variability or other sources of uncertainty are not taken into account, thus the inherent dispersion in the response of the building is neglected. Considering all these, an assessment step is necessary and a re-design step may possibly be needed as it is not guaranteed that all the targeted POs will be met at first pass. Still, by using only one step, a near-final design of the building is achieved, which can be easily improved in a subsequent iteration. More accurate methods, which allow consideration of the complete hazard of the site, the dispersion in demand observed in nonlinear dynamic analyses and the effect of uncertainties are also available at the cost of needing more initial input data (Vamvatsikos and Aschheim [27]).

Acknowledgments

The first author gratefully acknowledge the financial support provided by the Ministery of Education of Spain with a Salvador de Madariaga grant. The work of the second author was partially supported by the Eugenides Foundation and by the EU Innovation and Networks

Executive Agency (INEA) under the Horizon 2020 program PANOPTIS, Grant Agreement number 769129.

References

[1] Kurama, Y. C., Pessiki, S., Sause, R., and Lu, L.-W. (1999). “Seismic behavior and design of unbonded posttensioned precast concrete walls.” PCI J., 44(3), 72–89.

[2] Pérez, F.J., Sause R. and Pessiki S.(2007). "Analytical and Experimental Lateral Load Behavior of Unbonded Posttensioned Precast Concrete Walls". J. Struct.Eng. 133(11): 1531-1540.

[3] Hassanli R, ElGawady M A and Mills J E (2016). " Force–displacement behavior of unbonded post-tensioned concrete walls". Engineering Structures, 106, 495-505.

[4] Aaleti S and Sritharan S (2009). "A simplified analysis method for characterizing unbonded post-tensioned precast wall systems". Engineering Structures, 31 (12), 2966-2975.

[5] PEER Report 2011/104. Design and Instrumentation of the 2010 E-Defense Four-Story Reinforced Concrete and Post-Tensioned Concrete Buildings.

[6] Aschheim, M. A., Black, E. F. “Yield point spectra for seismic design and rehabilitation,” *Earthquake Spectra*, EERI, 2000; 16(2): 317-335.

[7] Priestley M. J. N., Calvi G.M and Kowalsky M.J. Displacement-Based Seismic Design of Structures, IUSS Press, Pavia. 2007.

[8] Eurocode 8: Design of structures for earthquake resistance -part 1: General rules, seismic actions and rules for buildings. EN1998-1. Brussels: European Committee for Standardization, April, 2004.

[9] Eurocode 2: Design of concrete structures—part 1: General rules and rules for buildings prEN 1992-1-1. Brussels: European Committee for Standardization, July 2002.

[10] Mander, J. B., Priestley, M. J. N., and Park, R. (1988). “Theoretical stress-strain model for confined concrete.” J. Struct. Eng., 114 (8), 1804–1826.

[11] SeismoStruct (2016). www.seismosoft.com.

[12] Cornell CA, Jalayer F, Hamburger RO, Foutch DA (2002). The probabilistic basis for the 2000 SAC/FEMA steel moment frame guidelines. ASCE Journal of Structural Engineering, 128(4), 526–533.

[13] Vamvatsikos D. (2017). Performance-based seismic design in real life: The good, the bad and the ugly. Proceedings of the ANIDIS2017 Italian National Conference on Earthquake Engineering, Pistoia, Italy.

[14] ASCE (2010). Minimum Design Loads for Buildings and Other Structures”, Standard ASCE/SEI 7–10. American Society of Civil Engineers, Reston, VA.

[15] McKenna, F., Fenves, G. L., & Scott, M. H. (2000). Open system for earthquake engineering simulation. University of California, Berkeley, CA.

[16] Buddika, H. S., & Wijeyewickrema, A. C. (2016). Seismic performance evaluation of posttensioned hybrid precast wall-frame buildings and comparison with shear wall-frame buildings. Journal of Structural Engineering, 142(6), 04016021.

[17] Calabrese A., Almedia J.P., Pinho R. (2010). Numerical issues in distributed inelasticity modeling of RC frame elements for seismic analysis. Journal of Earthquake Engineering, 14(S1):38–68.

[18] JCSS (2001). Probabilistic Model Code, Part III - Resistance Models, Joint Committee on Structural Safety. http://www.jcss.byg.dtu.dk/Publications/Probabilistic_Model_Code

[19] Vamvatsikos, D., & Cornell, C. A. (2002). Incremental dynamic analysis. Earthquake Engineering & Structural Dynamics, 31(3), 491-514.

[20] FEMA (2009). Quantification of Building Seismic Performance Factors. FEMA P-695, prepared by the Applied Technology Council for the Federal Emergency Management Agency, Washington, D.C.

[21] Luco N, Bazzurro P. (2007). Does amplitude scaling of ground motion records result in biased nonlinear structural drift responses? Earthquake Engineering and Structural Dynamics, 36(13):1813–1836.

[22] Baker JW, Cornell CA. 2006. Spectral shape, epsilon and record selection. Earthquake engineering and structural dynamics, 35(9):1077–1095.

[23] Lin T, Haselton CB, Baker JW. (2013). Conditional spectrum-based ground motion selection. Part I: Hazard consistency for risk-based assessments. Earthquake Engineering and Structural Dynamics, 42(12):1847–1865.

[24] Kazantzi A.K., Vamvatsikos D. (2015). Intensity measure selection for vulnerability studies of building classes. Earthquake Engineering and Structural Dynamics, 44(15): 2677–2694.

[25] Adam C., Kampenhuber D., Ibarra L.F., Tsantaki S. (2017). Optimal Spectral Acceleration-based Intensity Measure for Seismic Collapse Assessment of PDelta Vulnerable Frame Structures, Journal of Earthquake Engineering, 21:7, 1189-1195.

[26] Kohrangi M., Bazzurro P., Vamvatsikos D., Spillatura A. (2017). Conditional spectrum based ground motion record selection using average spectral acceleration. Earthquake Engineering and Structural Dynamics, 46(10):1667-1685.

[27] Vamvatsikos, D., & Aschheim, M. A. (2016). Performance-based seismic design via yield frequency spectra. Earthquake Engineering & Structural Dynamics, 45(11), 1759-1778.